Numerical grid methods for quantum-mechanical scattering problems

T. N. Rescigno[1,2] and C. W. McCurdy[2,3]
[1]*Physics Directorate, Lawrence Livermore National Laboratory, Livermore, California 94551*
[2]*Computing Sciences Directorate, Lawrence Berkeley National Laboratory, Berkeley, California 94720*
[3]*Department of Applied Science, University of California, Davis, Livermore, California 94551*
(Received 16 February 2000; published 11 August 2000)

We show how the finite-element method can be implemented using a discrete variable representation to provide an efficient means for directly solving the time-independent Schrödinger equation on a multidimensional numerical grid. For collision problems, an exterior complex scaling transformation obviates the need for explicit imposition of asymptotic boundary conditions, making the method particularly useful for studying three-body breakup. The method is illustrated by studying an analytically solvable two-dimensional (2D) breakup problem as well as a 2D model problem with exponential potentials.

PACS number(s): 34.80.Dp, 03.65.Nk

I. INTRODUCTION

Although analytic basis set expansions have traditionally been used in constructing solutions of the Schrödinger equation for both bound and continuum states, direct numerical solution with grid-based methodologies offers several distinct advantages and continues to increase in popularity. Finite difference methods are perhaps the simplest to implement, but generally require high-order difference formulas and/or very small grid spacings to achieve an acceptable level of accuracy. Finite-element methods [1], which employ basis functions that have compact support, offer more rapid convergence and numerical stability with larger grid spacings. While both methods generally lead to sparse, structured matrices that are well suited to iterative methods of solution, finite-element methods require the computation of potential matrix elements, which can be computationally intensive for multidimensional problems.

The discrete variable representation [2] refers to a class of methods that avoid the necessity of calculating complicated matrix elements. The discrete variable representation (DVR) in a sense provides a link between analytic basis set methods, which discretize the wave function in function space, and pure grid methods, which discretize the wave function in physical space. The attractive feature of the DVR is that the potential matrix elements are diagonal and equal to the potential values at the grid points, while the matrix elements of the kinetic energy have simple analytic forms. Thus the DVR preserves many of the features of finite difference methods without having to resort to numerical approximation of derivatives. In the DVR, the kinetic-energy matrix is generally full, so the bandwidth of the resulting linear equations is typically larger than it is with finite difference methods.

When applying any of these methods to collision problems, an important aspect of the implementation is the treatment of asymptotic boundary conditions. This is particularly difficult in collisions that involve three-body breakup, where energy can be shared continuously between the final collision fragments, since the boundary conditions are complicated and difficult to apply. In recent work [3,4], we have shown that the imposition of asymptotic boundary conditions can be avoided by applying an *exterior complex scaling* transformation to the equation that describes the outgoing wave portion (scattered wave) of the continuum wave function. Exterior complex scaling (ECS) is a generalization of uniform complex scaling [5] in which all interparticle distances are scaled by a complex number. The scattered wave falls off exponentially under such a transformation, just like the wave function for an ordinary bound state. ECS [6] was introduced as a logical extension of uniform scaling to deal with potentials that may have interior nonanalyticities or that may only be known numerically in a part of the entire coordinate space. Under ECS, the coordinates are complex scaled, but only outside a hypersphere of radius R_0, so that the scattered wave again falls off exponentially, but only beyond the hypersphere radius. While most applications of complex scaling have focused on the determination of the energies and lifetimes of autoionizing states, we have shown that ECS can also be used to compute collision cross sections, particularly in cases where the asymptotic boundary conditions make traditional scattering methods difficult to apply. The idea is to solve the transformed Schrödinger equation on a grid that extends far enough past R_0 that the scattered wave can be safely set to zero. By making R_0 large enough to enclose the entire interaction region, the collision dynamics can be extracted from the physical region inside the hypersphere where the coordinates are real. This method has been implemented for electron-hydrogen scattering using both finite elements [3,4] and finite difference [7] and has in fact produced essentially exact results for electron-impact ionization of hydrogen [8].

Our purpose here is to examine the use of ECS in the context of the discrete variable representation. When implementing complex scaling in the context of a basis set expansion, some care must be taken to account for the metric (Jacobian) that accompanies the scaling operator [9]. For uniform scaling, the metric is just a constant phase factor, which is easily incorporated into the kinetic- and potential-energy matrix elements that define the Hamiltonian. For exterior complex scaling, the Jacobean that defines the transformation is discontinuous at R_0, and the derivative of the wave function changes discontinuously at R_0 as well. Such cusp discontinuities are difficult to accommodate with analytic basis functions. One remedy for this problem is to smooth the transition from the inner unscaled to the outer scaled region over a finite interval. This remedy is not en-

tirely satisfactory: in addition to complicating the evaluation of matrix elements, it introduces an element of uncertainty into numerical computations, giving rise to errors that can depend sensitively on the way in which the contours are smoothed. Nevertheless, ''smooth exterior scaling'' has been made to work in a number of applications [9–11]. Karlsson [12], in particular, has shown how to implement exterior complex scaling for the DVR via a general coordinate mapping.

We will show below that it is possible to combine finite elements with the DVR. This makes it possible to implement exterior complex scaling without the need for smoothing the rotation contour. Combining the finite-element method (FEM) and DVR, moreover, allows one to combine the most desirable features of each method—the sparse, structured matrices of the FEM and the diagonal representation of the potential produced by the DVR are combined in a single method. This should make the proposed method useful in other applications that do not necessarily involve exterior complex scaling.

II. FINITE ELEMENTS AND THE DISCRETE VARIABLE REPRESENTATION

In the finite-elements method, the wave function is not expanded in terms of global functions. Rather, each independent variable r is replaced by a grid of nodes $0 \leqslant r_1 < r_2 < \cdots < r_N$, and a set of linearly independent local functions is used to represent the wave function in each interval. Elementary finite-element basis functions $f_{i,m}(r)$ are defined to be identically zero outside a given interval

$$f_{i,m}(r)=0, \quad r \notin [r_i, r_{i+1}], \quad i=1,\cdots,N, \quad m=1,n. \tag{1}$$

The index m is used to delineate the local basis functions in each interval as well as the boundary conditions imposed on the basis functions at the nodes. We will assume that the $f_{i,m}(r)$ satisfy the following conditions:

$$\begin{aligned} f_{i,1}(r_i)&=1, \\ f_{i,n}(r_{i+1})&=1, \\ f_{i,m}(r_i)=f_{i,m}(r_{i+1})&=0, \quad \text{otherwise.} \end{aligned} \tag{2}$$

For multidimensional problems, we use products of one-dimensional functions to expand the wave function.

The wave function must be continuous across each nodal boundary. We can turn this condition into a simple constraint on the expansion coefficients $c_{i,m}$ by requiring

$$c_{i,n}=c_{i+1,1}. \tag{3}$$

Equivalently, we can start with the set of $n \times N$ elementary functions and form a smaller set of $(n-1)\times N+1$ basis functions on which to project the Hamiltonian by combining each pair of elementary functions $f_{i,n}$ and $f_{i+1,i}$ into a single continuous function.

The foregoing description of the FEM is quite general and makes no assumptions about the specific form of the elementary basis functions. When a local polynomial basis is chosen, as is the case in most applications, it is also possible to impose continuity conditions on the derivatives of the wave function at the nodal boundaries by appropriate definition of the elementary functions. For example, we have previously employed fifth-order Hermite interpolating polynomials as the elementary basis [3,9], which allows us to impose continuity conditions on the wave functions as well as on its first and second derivatives. However, these additional constraints are not formally needed and, by requiring only the conditions contained in Eq. (2), we are free to explore a DVR implementation of the finite-element method, which we describe next.

The discrete variable representation uses a discretization procedure that is analogous to employing ''a basis of grid points'' in which local potential operators are represented as diagonal matrices. This is accomplished by starting from a polynomial basis that is connected to a Gauss quadrature rule and using that quadrature rule in evaluating all overlap and Hamiltonian matrix elements. To see how the DVR can be used in connection with the FEM, we begin with the grid defined by the FEM nodes and further subdivide each interval with a set of Gauss quadrature points $\{x_m^i\}$, $m=1\cdots n$. Since we will still want to impose continuity conditions at the endpoints of each interval, we follow Manolopoulos and Wyatt [13] in choosing a quadrature that constrains the endpoints of each interval to be included as quadrature points. This constraint is incorporated into the definition of the so-called Gauss-Lobatto quadrature points and weights.

Gauss-Lobatto quadrature is similar to the more familiar Gauss-Legendre quadrature, both of which approximate integrals as

$$\int_{-1}^{1} g(x)dx \cong \sum_{m=1}^{n} g(x_m)w_m. \tag{4}$$

In Gauss-Legendre quadrature, the points and weights $[x_i, w_i]$ are chosen to make Eq. (4) exact when $g(x)$ is a polynomial of degree $\leqslant 2n+1$. Equation (4) can be generalized to treat definite integrals over an arbitrary interval by scaling the points and weights:

$$\int_{r_i}^{r_{i+1}} g(x)dx \cong \sum_{m=1}^{n} g(x_m^i)w_m^i, \tag{5}$$

where

$$\begin{aligned} w_m^i &= \frac{(r_{i+1}-r_i)}{2} w_m, \\ x_m^i &= \tfrac{1}{2}[(r_{i+1}+r_i)x_m + (r_{i+1}-r_i)]. \end{aligned} \tag{6}$$

In Gauss-Lobatto quadrature [14], two of the points are constrained to coincide with the endpoints, $x_1^i = r_i$ and $x_n^i = r_{i+1}$. The weights and remaining points are chosen to make Eq. (5) exact for polynomials of degree $\leqslant 2n-1$:

$$\int_{r_i}^{r_{i+1}} g(x)dx \cong g(r_i)w_1^i + \left[\sum_{m=2}^{n-1} g(x_m^i)w_m^i\right] + g(r_{i+1})w_n^i . \tag{7}$$

To construct a DVR based on Gauss-Lobatto quadrature, we choose the elementary basis functions to be Lagrange interpolating polynomials or, as Manolopoulos and Wyatt [13] call them, Lobatto shape functions:

$$f_{i,m}(x) = \prod_{j\neq m} \frac{(x-x_j^i)}{(x_m^i - x_j^i)}, \quad r_j \leqslant x \leqslant r_{i+1}$$

$$= 0, \quad x < r_i, x > r_{i+1}. \tag{8}$$

The Lobatto shape functions have the property that

$$f_{i,m}(x_{m'}^{i'}) = \delta_{i,i'}\delta_{m,m'}, \tag{9}$$

and thus clearly satisfy the conditions of Eq. (2). Moreover, if we use the Gauss quadrature rule Eq. (7) to approximate all required integrals, then it follows that the functions are orthogonal in the sense of the Lobatto quadrature

$$\int_0^\infty f_{im}(x) f_{i'm'}(x)dx = \delta_{ii'} \int_{r_i}^{r_{i+1}} f_{im}(x) f_{im'}(x)dx$$

$$\cong \delta_{ii'} \sum_{j=1}^{n} f_{im}(x_j^i) f_{im'}(x_j^i) w_j^i$$

$$= \delta_{ii'}\delta_{mm'} w_m^i, \tag{10}$$

and that any local operator has a diagonal representation:

$$\int_0^\infty f_{im}(x) V(x) f_{i'm'}(x)dx \cong \delta_{ii'}\delta_{mm'} V(x_m^i) w_m^i . \tag{11}$$

To insure continuity of the wave function at the interval boundaries, we combine the two Lobatto shape functions $f_{i,n}$ and $f_{i+1,1}$, which are both unity at r_{i+1}, into a single ''bridge'' function that we denote χ_{i1}. The basis in which the wave function is expanded is thus defined as

$$\chi_{i1}(x) = f_{i,n}(x) + f_{i+1,1}(x),$$
$$\chi_{im}(x) = f_{i,m}(x), \quad m = 2, \cdots, n-1. \tag{12}$$

The bridge functions guarantee continuity of the wave function at the interval boundaries. If it were not for these bridge functions, there would be no coupling between basis functions in adjacent intervals. Boundary conditions that the wave function vanish at $x=0$ and $x=r_N$ are imposed by simply deleting the functions f_{11} and f_{Nn} from the basis. The total number of basis functions would then be $(n-1)\times N - 1$. The basis functions we have defined are orthogonal [in the sense of Eq. (10)], but not normalized. A normalized basis [in the sense of Eq. (10)] is obtained by using

$$\chi_{i,m}(x) \equiv f_{i,m}(x)/\sqrt{w_m^i}, \quad m = 2, n-1,$$
$$\chi_{i,1}(x) \equiv (f_{i,n}(x) + f_{i+1,1}(x))/\sqrt{w_n^i + w_1^{i+1}}. \tag{13}$$

A wave function that is expanded in terms of basis functions defined in Eq. (13) will be continuous at the finite-element boundaries, but need not have continuous derivatives [15]. As a result, some care is needed in defining the kinetic-energy matrix elements. Here we follow Scrinzi and Elander [16], who point out that the derivative of the wave function need not be continuous to correctly define the kinetic energy. Consider a function $\psi(x)$ whose derivative is discontinuous at the point x_0, that is,

$$d\psi(x)/dx = f(x)\,\theta(x-x_0) + g(x)\,\theta(x_0 - x), \tag{14}$$

where $\theta(x)$ is the step function

$$\theta(x) = \begin{cases} 0, & x<0 \\ 1, & x>0. \end{cases} \tag{15}$$

The proper definition of the second derivative of such a function, when used under an integral, is

$$d^2\psi(x)/dx^2 = f'(x)\,\theta(x-x_0) + g'(x)\,\theta(x_0-x)$$
$$+ (f(x) - g(x))\,\delta(x-x_0). \tag{16}$$

Now consider the case of a one-dimensional (1D) (radial) wave function that is expanded as

$$\psi(x) = \sum_{i,m} c_{i,m}\chi_{i,m}(x). \tag{17}$$

By using Eqs. (14)–(16) in each term of Eq. (17), the expectation value of the radial kinetic energy can be expressed in symmetric form as

$$-\tfrac{1}{2}\int_0^\infty dx\,\psi(x)\frac{d^2}{dx^2}\psi(x) = -\tfrac{1}{2}\lim_{\varepsilon\to 0}\sum_i \int_{r_i+\varepsilon}^{r_{i+1}-\varepsilon} dx\;\psi(x)$$
$$\times \sum_m c_{i,m}\chi''_{i,m}(x)$$
$$-\tfrac{1}{2}\int_0^\infty dx\;\psi(x)\sum_{i,m} c_{i,m}\delta(x-r_i)$$
$$\times [\chi'_{i,m}(r_i+0) - \chi'_{i,m}(r_i-0)]$$
$$= \tfrac{1}{2}\sum_i \int_{r_i}^{r_{i+1}} dr\,(d\psi/dr)^2. \tag{18}$$

This result is obtained by integrating by parts and noting that the δ-function terms precisely cancel the surface terms that come from the finite-element boundaries. Note that any finite value of ε allows us to segregate the finite terms in Eq. (18) from the δ-function terms. Thus the kinetic-energy matrix elements in our FEM-DVR are evaluated as

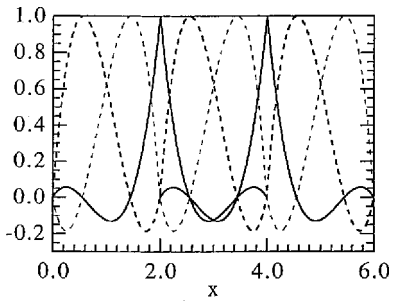

FIG. 1. Lobatto shape functions for finite-element calculations. Basis functions are shown for the case where there are three elements and $n=4$ in each element. The solid curves show the ''bridge'' functions that link adjacent elements.

$$T^{i,i'}_{m,m'} \equiv \tfrac{1}{2}(\delta_{i,i'} + \delta_{i,i'\pm 1}) \int_0^\infty dx \frac{d}{dx}\chi_{i,m}(x) \frac{d}{dx}\chi_{i',m'}(x), \tag{19}$$

with the δ-functions reflecting the fact that there is no overlap between basis functions beyond adjacent intervals.

Although matrix elements of the kinetic-energy operator are not diagonal in the DVR, they are given by simple analytic formulas when evaluated by using the Gauss quadrature rule. The required elements are simply evaluated in terms of the first derivatives of the Lobatto shape functions at the quadrature points, which are given by [13]

$$f'_{im}(x^i_{m'}) = \frac{1}{(x^i_m - x^i_{m'})} \prod_{k\neq m,m'} \frac{(x^i_{m'} - x^i_k)}{(x^i_m - x^i_k)}, \quad m \neq m'$$

$$= \frac{1}{2w^i_m}(\delta_{m,n} - \delta_{m,1}), \quad m = m'. \tag{20}$$

The simplicity of the matrix elements in the DVR and the orthonormality of the basis derives solely from the use of the Gauss quadrature rules to approximate the integrals. It is important to remember, however, that the Lobatto shape functions have an underlying continuous representation [Eq. (8)] that can be used to evaluate the wave function at arbitrary points, once the expansion coefficients are known.

Using Lobatto shape functions in connection with finite elements gives one considerably flexibility in tailoring the grid to a specific problem, since we are free to place the finite-element boundaries arbitrarily and to use different order quadratures in each element, if so desired. Moreover, since basis functions in one element are only connected to those in an adjacent element through a single bridge function, the Hamiltonian matrix can be made quite sparse. We plot the Lobatto shape functions in Fig. 1 for the case where there are only three elements and we use $n=4$ in each element.

It is interesting to see how this FEM-DVR scheme scales compared to a traditional DVR that would span the range of each independent variable with a single element. In both methods, the number of nonzero Hamiltonian matrix elements is determined only by the kinetic-energy operator, since the potential is fully diagonal in DVR. (This is of course not true in a traditional FEM method and is the major advantage of using DVR in multidimensional problems.) In traditional DVR, the 1D kinetic energy is a full $N\times N$ matrix with N^2 nonzero elements, where N is the number of DVR functions. In FEM-DVR, we decompose N into M elements with n DVR functions per element, $N=M\times n$, so the number of nonzero kinetic-energy elements is $\sim M\times n^2$. For a N_D-dimensional problem, if we use a product basis and assume that the kinetic energy is a sum of 1D operators, then the number of nonzero matrix elements is $N_D\times N^{N_D-1}\times N^2$ for traditional DVR and $N_D\times N^{N_D-1}\times m\times n^2$ with FEM-DVR. The ratio of nonzero elements in the two schemes is thus N/n, independent of the number of dimensions

In multidimensional problems, the bulk of the computational time in DVR methods will be spent on solving the linear equations and the scaling will depend on details of the specific algorithms used. In our work here on two-dimensional (2D) problems, we used a sparse linear equation solver whose time scaled roughly as the number of nonzero elements to the $\frac{3}{2}$ power. We generally decomposed our grids into nine finite elements, which means that we gained approximately a factor of 27 speedup over what we would have needed in a traditional DVR method.

III. EXTERIOR COMPLEX SCALING

Under exterior complex scaling, the coordinates are transformed under the mapping [6]

$$R(r) = \begin{cases} r, & r < R_0 \\ R_0 + (r-R_0)e^{i\phi}, & r \geqslant R_0 \end{cases}. \tag{21}$$

Under this transformation, any function F that behaves like a pure outgoing wave at large distances, i.e.,

$$F(r) \underset{r\to\infty}{\sim} Ae^{ikr} \tag{22}$$

will decrease exponentially as $r\to\infty$. ECS can therefore be used in quantum-scattering applications to avoid explicit enforcement of asymptotic boundary conditions by applying the transformation to the equation that determines the outgoing part of the full wave function [3,4]. If the full wave function is expressed as the sum of an unperturbed initial state and a scattered wave part

$$\Psi^+ = \Phi_0 + \Psi_{\rm sc}, \tag{23}$$

then it is easy to show that the scattered wave satisfies an inhomogeneous Schrödinger equation:

$$(E-H)\Psi_{\rm sc} = (H-E)\Phi_0, \tag{24}$$

which can be discretized using the FEM-DVR methods just outlined. The ECS transformation is applied to the finite-element boundaries $[r_i]$, making sure that the exterior scaling radius R_0 coincides with one of the nodes, r_I:

$$R_i=\begin{cases} r_i, & i<I \\ r_I+(r_i-r_I)e^{i\phi}, & i\geqslant I. \end{cases} \tag{25}$$

This defines a segmented coutour of points that are real out to R_0 and then fall on a complex ray. The DVR quadrature points and weights can then be determined for each segment of the contour; the points and weights belonging to elements $i\geqslant I$ will of course be complex:

$$\chi_{i,m}\equiv f_{i,m}(R(x))/\sqrt{e^{i\phi}w_m^i}, \quad m=2,n-1, \quad i\geqslant I, m\neq 1$$

$$\chi_{i,1}\equiv[f_{i,n}(R(x))+f_{i+1,1}(R(x))]/\sqrt{e^{i\phi}(w_n^i+w_1^{i+1})}, \quad i>I. \tag{26}$$

In particular, the complex bridge function centered at $R_0=R_I$,

$$\chi_{I,1}\equiv[f_{I,n}(x)+f_{I+1,1}(R(x))]/\sqrt{w_n^I+e^{i\phi}w_1^{I+1}}, \tag{27}$$

guarantees continuity of the scattered wave at the exterior scaling radius. This contrasts markedly from the procedure proposed by Karlsson [12], who used DVR without the requirement that R_0 coincide with an endpoint. In that case, a smooth mapping from real to complex coordinates must be employed, which entails additional complications [9,12]. By contrast, we have found no numerical difficulties associated with the use of sharp exterior scaling in the FEM-DVR procedure just outlined.

IV. NUMERICAL EXAMPLES

To illustrate the techniques we have just outlined, we consider several 2D model problems involving two particles of the mass of an electron, with zero angular momentum, interacting with each other and a center of force. We employ atomic units $(m=e=\hbar=1)$ throughout.

The first example, which we have previously studied in a different context [17], is a problem for which an analytic solution is obtainable, thus providing a rigorous test of the proposed numerical method. We consider a hypothetical breakup problem in which the free-particle Green's function governs the motion of the scattered wave. The Green's function for two free particles is defined by the equation

$$[E+\tfrac{1}{2}\nabla_1^2+\tfrac{1}{2}\nabla_2^2]G(\mathbf{r}_1,\mathbf{r}_2;\mathbf{r}_1',\mathbf{r}_2';E)=\delta(\mathbf{r}_1-\mathbf{r}_1')\,\delta(\mathbf{r}_2-\mathbf{r}_2'). \tag{28}$$

The outgoing-wave solution for this problem can be expressed in closed form as [18]

$$G(\mathbf{r}_1,\mathbf{r}_2;\mathbf{r}_1',\mathbf{r}_2';E)=-\frac{iK^2}{8\pi^2}\frac{H_2^{(1)}(K|\rho-\rho'|)}{|\rho-\rho'|^2}, \tag{29}$$

where $E=K^2/2$, $H_2^{(1)}$ is a Hankel function of integer order 2 and ρ is the six vector:

$$\rho=\begin{bmatrix}\mathbf{r}_1\\ \mathbf{r}_2\end{bmatrix}. \tag{30}$$

We want the Green's function for s waves, which is obtained from Eq. (29) by taking the matrix element

$$\frac{G(r_1,r_2;r_1',r_2';E)}{r_1r_2r_1'r_2'}=\int Y_{00}^*(\Omega_1)Y_{00}^*(\Omega_2)\times G(\mathbf{r}_1,\mathbf{r}_2;\mathbf{r}_1',\mathbf{r}_2';E)Y_{00}(\Omega_1')\times Y_{00}(\Omega_2')d\Omega_1d\Omega_2d\Omega_1'd\Omega_2'. \tag{31}$$

The integrations can be performed by using the identity

$$\frac{\partial\partial}{\partial x\partial y}H_0^{(1)}((a-bx-cy)^{1/2})=bc\frac{H_2^{(1)}((a-bx-cy)^{1/2})}{4(a-bx-cy)} \tag{32}$$

to derive the result

$$\begin{aligned}G(r_1,r_2;r_1',r_2';E)=-\frac{i}{2}\{&H_0^{(1)}[K((r_1^2+r_1'^2)+(r_2^2+r_2'^2))^{1/2}]\\&-H_0^{(1)}[K((r_1^2-r_1'^2)+(r_2^2+r_2'^2))^{1/2}]\\&-H_0^{(1)}[K((r_1^2+r_1'^2)+(r_2^2-r_2'^2))^{1/2}]\\&+H_0^{(1)}[K((r_1^2-r_1'^2)+(r_2^2-r_2'^2))^{1/2}]\}.\end{aligned} \tag{33}$$

If we switch to hyperspherical coordinates, $r_1=\rho\sin\alpha$, $r_2=\rho\cos\alpha$, and use the asymptotic form of the Hankel function

$$H_0^{(1)}(z)\rightarrow e^{-i\pi/4}\left(\frac{2}{\pi}\right)^{1/2}\frac{e^{iz}}{z^{1/2}}, \tag{34}$$

we get the limiting behavior of $G(r_1,r_2;r_2',r_2';E)$ for large ρ:

$$G(r_1,r_2;r_1',r_2';E)\underset{\rho\rightarrow\infty}{\sim}-e^{-i3\pi/4}2\left(\frac{2}{\pi}\right)^{1/2}\frac{e^{iK\rho}}{(K\rho)^{1/2}}\times\sin[K\sin(\alpha)r_1]\sin[K\cos(\alpha)r_2']. \tag{35}$$

We now consider a hypothetical problem in which the scattered wave is determined by the equation:

$$\left(E+\frac{1}{2}\frac{d^2}{dr_1^2}+\frac{1}{2}\frac{d^2}{dr_2^2}\right)\Phi(r_1,r_2)=\phi_0(r_1,r_2) \tag{36}$$

or

$$\Phi(r_1,r_2)=\int\int G(r_1,r_2;r_1',r_2';E)\,\phi_0(r_1',r_2')dr_1'dr_2', \tag{37}$$

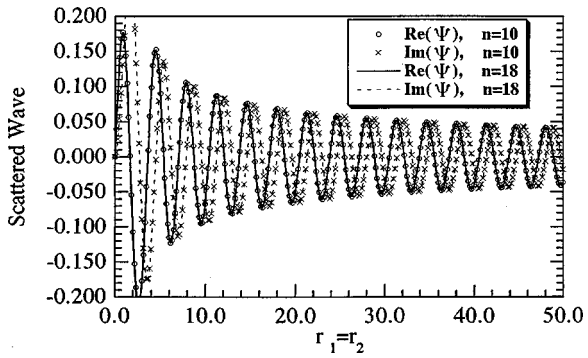

FIG. 2. Real part of the scattered wave along the diagonal ($r_1=r_2$) for the model problem discussed in text. The total energy is 24 eV and the real portion of the grid extends to 50 bohrs in each radial dimension. The solid line is the result obtained using $n=18$ and the points correspond to $n=10$.

where $\phi_0(r_1,r_2)$ is chosen to be a simple product of exponentials:

$$\phi_0(r_1,r_2)=e^{-r_1}e^{-r_2}. \tag{38}$$

With this choice, we can use the asymptotic form for G given in Eq. (35) to perform the integration in Eq. (37) analytically and get an expression for $\Phi(r_1,r_2)$ that is valid for large ρ:

$$\Phi(r_1,r_2) \underset{\rho\to\infty}{\sim} -e^{-i3\pi/4}\,2\left(\frac{2}{\pi}\right)^{1/2}\frac{e^{iK\rho}}{(K\rho)^{1/2}}\left(\frac{K\sin\alpha}{1+K^2\sin^2\alpha}\right) \times\left(\frac{K\cos\alpha}{1+K^2\cos^2\alpha}\right). \tag{39}$$

For small values of r_1 and r_2, the integrations in Eq. (37) must be performed numerically using the exact Green's function given in Eq. (33).

We used the foregoing expressions to test the accuracy of our proposed FEM-DVR scheme. We solved Eq. (36) on a 2D numerical grid, expanding Φ as

$$\Phi(r_1,r_2)=\sum_{i,m,j,n} c_{i,m}^{j,n}\chi_{i,m}(r_1)\chi_{j,n}(r_2). \tag{40}$$

For each radial coordinate, we used nine finite elements with a nodal spacing of 10 bohrs and varied the number of DVR basis functions n in each element. The rotation angle for the ECS transformation was set at 30° and R_0 was set at 50 bohrs. Convergence of the wave function to six figures over the entire real portion of the grid was achieved with a value of $n=18$, corresponding to a total number of 152 DVR functions in each radial dimension. Convergence with respect to n was quite rapid. Figure 2 compares the computed values of the wave function at $E=24$ eV ($K=1.328$) along the diagonal ($r_1=r_2$) using values of $n=10$ and $n=18$.

We have argued that combining FEM with DVR avoids any numerical difficulties associated with the use of sharp exterior scaling. To test this hypothesis, we performed a second set of calculations, moving R_0 from 50 to 60 bohrs.

TABLE I. Convergence of the wave function at $r_1=r_2=50$ bohrs for the model problem discussed in text at $E=24$ eV. n is the number of the Lobatto shape functions used in each radial finite element. The finite-element nodal spacing is 10 bohrs. Results are given for two different values of R_0 in the exterior complex scaling transformation.

n	$R_0=50$	$R_0=60$
8	(−.020 621 9, −.016 469 7)	(−.019 182 4, −.011 639 5)
9	(−.033 986 3, −.029 580 6)	(−.036 486 0, −.025 567 6)
10	(−.037 988 9, −.017 222 4)	(−.037 759 1, −.017 673 5)
12	(−.036 725 5, −.018 304 2)	(−.036 722 3, −.018 311 0)
14	(−.036 713 1, −.018 321 1)	(−.036 713 1, −.018 321 2)
16	(−.036 713 1, −.018 321 2)	(−.036 713 1, −.018 321 2)
18	(−.036 713 1, −.018 321 2)	(−.036 713 1, −.018 321 2)

Table I compares values of the wave function at at $r_1=r_2=50$ bohrs as a function of n from calculations with R_0 set at 50 and 60 bohrs. In both cases, the wave function converges rapidly to the correct value. There was evidently no problem with convergence caused by the discontinuous change in slope in the ECS contour at R_0, which is easily handled with finite elements.

The second example is one we have also previously considered [17]. This problem is described by a Hamiltonian of the form

$$H=-\frac{1}{2}\frac{\partial^2}{\partial r_1^2}-\frac{1}{2}\frac{\partial^2}{\partial r_2^2}+V(r_1)+V(r_2)+W(r_1,r_2). \tag{41}$$

The one-body potentials V are attractive exponentials that bind only one state, $\varphi(r)$, with energy $-0.411\,45$ hartree:

$$V(r)=-3\exp(-r), \tag{42}$$

and the two-body potential is

$$W(r_1,r_2)=10\exp(-r_1-r_2). \tag{43}$$

We treat this problem with singlet spin coupling for the two electrons so that the initial state in Eqs. (23) and (24) is defined with symmetric permutational symmetry:

$$\Phi_0=\sin(k_0r_1)\varphi(r_2)+\sin(k_0r_2)\varphi(r_1), \tag{44}$$

where k_0 is the initial projectile momentum. These equations completely define the problem of solving Eq. (24) for the scattered wave, subject only to the boundary conditions that it is zero when $r_1=0$ or $r_2=0$ and purely outgoing. The latter condition is again imposed by using exterior complex scaling. To solve this problem, we used the same parameters for the exterior scaled FEM grid as in the previous example with $n=18$ DVR functions in each element. Figure 3 shows a plot of the real part of $\Psi_{sc}(r_1,r_2)$ for an incident energy of 30 eV($K=1.1756$) for $0\leqslant[r_1,r_2]\leqslant 50$ bohrs.

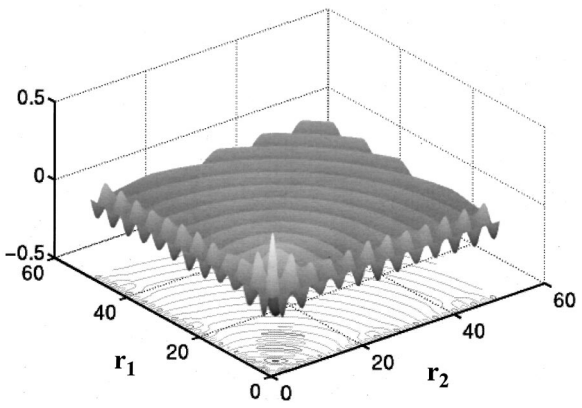

FIG. 3. Real part of the scattered wave function for model problem with short-range potentials at an incident energy of 30 eV. r_1 and r_2 are in bohr.

The total, elastic, and breakup cross sections are plotted in Fig. 4. The total cross section was obtained from the optical theorem

$$\sigma_{\rm tot} = -\frac{8\pi}{k^2}\,{\rm Im}\langle \Phi_0 | H - E | \Psi_{\rm sc}\rangle, \tag{45}$$

while the elastic cross section was obtained by using the ''projected optical theorem'' that we previously derived [3]:

$$\sigma_{\rm elastic} = -\frac{8\pi}{k^2}\,{\rm Im}\langle P\Psi_{\rm sc} | H_0 | P\Psi_{\rm sc}\rangle. \tag{46}$$

The operator P in Eq. (46) asymptotically projects out the target bound state:

$$P = |\varphi(r_1)\rangle\langle\varphi(r_1')| + |\varphi(r_2)\rangle\langle\varphi(r_2')|, \tag{47}$$

and H_0 is the total kinetic-energy operator. Since the target potential only binds one state, the breakup cross section is simply the difference between $\sigma_{\rm tot}$ and $\sigma_{\rm elastic}$. The values plotted in Fig. 4 agree with the results we previously obtained using a pure finite element method without the DVR [17].

We have also calculated the single-differential (energy-sharing) breakup cross section, which is conveniently defined using hyperspherical coordinates ρ and α in terms of the flux in the direction of ρ':

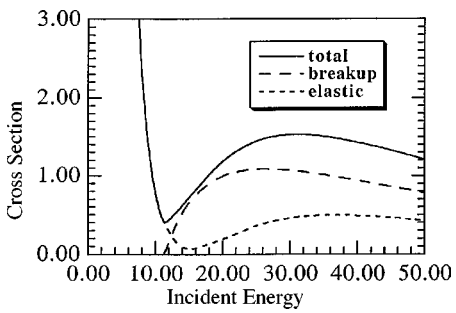

FIG. 4. Total, elastic, and breakup cross sections (in units of a_0^2) for short-range potential problem discussed in text. The incident energy is in eV.

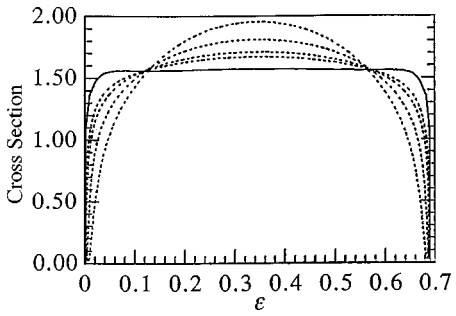

FIG. 5. Single-differential (energy-sharing) cross section (in units of a_0^2/hartree) for a short-range potential problem at an incident energy of 30 eV. The ejected particle energy ε_1 is plotted in hartrees. Dashed lines show values computed for ρ_0 values of 20, 30, 50, and 70 bohrs. Solid line is the value extrapolated to infinite ρ using $1/\rho$ behavior.

$$F(\rho_0,\alpha) = \frac{1}{2i}[(1-P)\Psi_{\rm sc}^*\nabla(1-P)\Psi_{\rm sc} - (1-P)\Psi_{\rm sc}\nabla(1-P)\Psi_{\rm sc}^*]_{\rho=\rho_0} \tag{48}$$

As $\rho_0 \to \infty$, the angle α also determines the ratio of the momenta of the two outgoing particles $\alpha = \tan^{-1}(k_1/k_2)$ and the single-differential cross section is calculated as

$$\frac{d\sigma(\varepsilon_1)}{d\varepsilon_1} = \frac{8\pi}{k_0^2 K^2 \sin\alpha\cos\alpha}\lim_{\rho_0\to\infty}[F(\rho_0,\alpha)\cdot\rho_0], \tag{49}$$

where $(2\varepsilon_1)^{1/2} = K\cos\alpha$ and $K^2/2 = E$. Note that by using projection operators in Eq. (48), we remove any contamination of the flux near $\alpha = 0$ and $\alpha = \pi/2$ arising from two-body elastic scattering [3,4]. Since the flux approaches its asymptotic limit as $1/\rho$ [4], it can easily be calculated by extrapolation from values obtained at several values of ρ_0. Figure 5 shows the energy-sharing breakup cross section for an incident energy of 30 eV for several values of ρ_0, along with the extrapolated value.

V. DISCUSSION

The discrete variable representation is widely used in chemical reaction dynamics because it greatly simplifies the matrix representation of the Hamiltonian. We have shown that the DVR can also be used in conjunction with the finite-element method to give a flexible and efficient numerical technique that is particularly well suited to numerical solutions of the Schrödinger equation for multidimensional problems. By combining the DVR with FEM, we retain the best features of both methods, i.e., the simple representation of the Hamiltonian that derives from the use of a DVR and the sparse, structured form of the Hamiltonian matrix that is a key feature of the FEM. We have shown how to implement this method by combining different polynomial bases of Lobatto shape functions into a set of continuous functions, thereby generalizing the method originally proposed by Manolopoulos and Wyatt [13].

We have also shown that exterior complex scaling can be

easily implemented with the proposed method, without the need for introducing smooth rotation contours or generalized coordinate mappings. Our principal interest is in the development of methods for studying electron-impact ionization, so we have emphasized applications that side-step the explicit imposition of asymptotic boundary conditions. The proposed numerical, techniques, however, should also prove useful in numerical studies of bound and resonance states as well as chemical reaction dynamics.

ACKNOWLEDGMENTS

This work was performed under the auspices of the U.S. Department of Energy by the Lawrence Berkeley National Laboratory and the Lawrence Livermore National Laboratory under Contract Nos. DE-AC03-76SF00098 and W-7405-Eng-48, respectively. The authors wish to acknowledge the use of computational resources of the National Energy Research Scientific Computing Center.

[1] D. H. Norrie and G. de Vries, *An Introduction to Finite Element Analysis* (Academic, New York, 1978).
[2] J. V. Lill, G. A. Parker, and J. C. Light, Chem. Phys. Lett. **89**, 483 (1982).
[3] C. W. McCurdy, T. N. Rescigno, and D. A. Byrum, Phys. Rev. A **56**, 1958 (1997).
[4] C. W. McCurdy and T. N. Rescigno, Phys. Rev. A **56**, R4369 (1977).
[5] For a review, see W. P. Reinhardt, Annu. Rev. Phys. Chem. **33**, 223 (1982).
[6] B. Simon, Phys. Lett. **71A**, 211 (1979).
[7] M. Baertschy, T. N. Rescigno, W. A. Isaacs, and C. W. McCurdy, Phys. Rev. A **60**, R13 (1999).
[8] T. N. Rescigno, M. Baertschy, W. A. Isaacs, and C. W. McCurdy, Science **286**, 2474 (1999).
[9] T. N. Rescigno, M. Baertschy, D. Byrum, and C. W. McCurdy, Phys. Rev. A **55**, 4253 (1997).
[10] N. Rom, E. Engdahl, and N. Moiseyev, J. Chem. Phys. **93**, 3413 (1990).
[11] N. Elander and E. Yarevsky, Phys. Rev. A **57**, 3119 (1998).
[12] H. O. Karlsson, J. Chem. Phys. **108**, 3849 (1998).
[13] D. E. Manolopoulos and R. E. Wyatt, Chem. Phys. Lett. **152**, 23 (1988).
[14] V. I. Krylov, *Approximate Calculation of Integrals* (MacMillan, New York, 1962).
[15] A. Scrinzi, Comput. Phys. Commun. **86**, 67 (1995).
[16] A. Scrinzi and N. Elander, J. Chem. Phys. **98**, 3866 (1993).
[17] T. N. Rescigno, C. W. McCurdy, W. A. Isaacs, and M. Baertschy, Phys. Rev. A **60**, 3740 (1999).
[18] E. Gerjuoy, Philos. Trans. R. Soc. London, Ser. A **270**, 197 (1971).